Journal of Materials Chemistry C

ROYAL SOCIETY OF CHEMISTRY

PAPER

View Article Online
View Journal

Cite this: DOI: 10.1039/d4tc01480d

Green solution synthesis of $Bi_{19}S_{27}I_3$ nanostructures – engineering their morphology through polyethylene glycol and their use in the photocatalytic reduction of Cr(VI)†

Maia Mombrú-Frutos,[a] Martina Viera,[ab] Carolina Grosso,[a] Mauricio Rodriguez Chialanza,[c] Laura Fornaro,[b] María Eugenia Pérez Barthaburu *[b] and Ivana Aguiar *[a]

Received 10th April 2024,
Accepted 20th August 2024

DOI: 10.1039/d4tc01480d

rsc.li/materials-c

Bismuth-based chalcohalides have garnered significant attention over the past five years due to their promising optoelectronic properties, and applicability in photodetection, ionizing radiation detection, photocatalysis, and solar cells. Among these compounds, $Bi_{19}S_{27}I_3$ stands out as a novel material with relatively unexplored synthesis and properties. In this study, we introduce a green synthesis approach for $Bi_{19}S_{27}I_3$ nanostructures, employing the hot injection method under mild conditions with water as the solvent. By utilizing polyethylene glycol (PEG) as a capping agent with molar proportions [PEG : Bi] 0.5 : 1, 1 : 1 and 2 : 1 and adjusting the reaction time (5 min or 270 min), we successfully controlled the morphology, yielding either round nanoparticles, nanorolls, or a combination of both. For instance, longer reaction times such as 270 min enhance the crystallinity of the material and also encourage morphology uniformity, while PEG favors a rounded morphology. Our findings underscore the significant capping effect of PEG, particularly evident in the photocatalytic activity of $Bi_{19}S_{27}I_3$ towards Cr(VI) reduction. Through this facile and efficient synthesis strategy, we tailored the morphology of $Bi_{19}S_{27}I_3$ and demonstrated its efficacy in Cr(VI) photocatalysis, achieving a remarkable 91% reduction for the nanoroll-based sample with PEG : Bi [1 : 1]. This innovative approach not only provides an environmentally friendly method for synthesizing $Bi_{19}S_{27}I_3$ but also highlights its potential as an effective photocatalyst for environmental remediation.

1. Introduction

Human activities generate multiple pollutants in water, presenting pressing challenges for clean water initiatives worldwide. Hexavalent chromium (Cr(VI)) contamination in water sources is a significant environmental and public health concern due to its toxicity and carcinogenicity.[1] Despite efforts to regulate its discharge, Cr(VI) persists as a pervasive pollutant, originating from industrial processes such as electroplating, leather tanning, and textile manufacturing.[2,3] Traditional remediation methods often fall short in effectively removing Cr(VI) from water systems, calling for the development of sustainable innovative approaches. Photocatalysis has emerged as a promising technology for addressing this challenge, harnessing the power of light-activated catalysts to degrade organic pollutants and transform toxic metal ions.[4]

In particular, the photocatalytic reduction of Cr(VI) to Cr(III) is a critical process in environmental remediation because of the significant differences in properties, such as toxicity, bioavailability and mobility, between these two species.[5] This reduction process has many advantages in the context of environmental remediation. For example, reduced toxicity; Cr(III) is significantly less toxic in aquatic habitats, thereby promoting healthier ecosystems and protecting biodiversity.[6] Additionally, it is an essential nutrient in trace amounts for human and animal metabolism.[7,8] The mobility of Cr(III) is lower as it tends to form hydroxides, thus precipitating in water bodies, helping to contain the contamination and to prevent further environmental damage.[9]

The photocatalytic reduction of Cr(VI) to Cr(III) can be considered as an environmentally friendly process that generally requires fewer chemicals and generates less secondary

[a] Área Radioquímica, Facultad de Química, Universidad de la República, Montevideo, Uruguay. E-mail: iaguiar@fq.edu.uy
[b] Departamento de Desarrollo Tecnológico, Centro Universitario Regional del Este, Universidad de la República, Rocha, Uruguay. E-mail: meperez@cure.edu.uy
[c] PDU Ciencias Físicas y sus Aplicaciones, Centro Universitario Regional del Este, Universidad de la República, Rocha, Uruguay

† Electronic supplementary information (ESI) available. See DOI: https://doi.org/10.1039/d4tc01480d

waste compared to conventional methods.[10] Thus, it is crucial for mitigating the adverse effects of chromium contamination and promoting cleaner and safer water resources.

Various types of nanomaterials have facilitated the photocatalytic reduction of Cr(VI) to Cr(III) in water, with inorganic semiconductors and graphitic carbon nitride (g-C_3N_4) emerging as the most widely employed materials.[11] Titanium dioxide exhibits high photocatalytic activity due to its suitable bandgap energy and strong oxidative potential. Its photocatalytic capabilities have been improved employing a variety of approaches, such as metal doping and combination with carbon-based materials.[12] However, one drawback of TiO_2 is its limited efficiency under visible light, necessitating the use of UV irradiation for optimal performance. Other metal-based semiconductors have been widely studied for the reduction of Cr(VI), pristine or in heterostructures, such as WO_3, ZnO, Ag_2S, Fe_2O_3, and Bi_2O_3 among others. However, the efficiency of these photocatalysts is not the best due to the rapid electron–hole pair recombination.[13] Graphitic carbon nitride, a metal-free semiconductor, has attracted attention for its visible-light responsiveness and chemical stability, making it a potential candidate for sustainable photocatalytic applications. However, its relatively low photocatalytic activity and challenges in synthesis scalability pose hurdles for widespread implementation.[14]

Bismuth based chalcohalides have been gaining exponential interest in the past five years, due to their optoelectronic properties, suitable for applications in photodetection,[15] ionizing radiation detection,[16] photocatalysis,[17] and solar cells.[18–20] They have been compared with halide perovskites, and proposed as more environmentally friendly and stable alternatives.[21] In particular, $Bi_{19}S_{27}I_3$ is a novel compound, whose synthesis and properties have not been thoroughly studied. $Bi_{19}S_{27}I_3$ is a ternary chalcohalide which crystallizes in the hexagonal space group $P6_3$. Due to having one bismuth atom in $\frac{1}{3}$ unit cell, the calculations to determine properties are very resource expensive. There is more than one way of writing its stoichiometry, and previous reports have named it $(Bi(Bi_2S_3)_9I_3)_{0.6667}$ (ref. 22) or $Bi_{13}S_{18}I_2$.[23] Most of the syntheses reported thus far make use of complicated metal–organic precursors such as bismuth xanthate that require pre-synthesis,[24] long reaction times,[23] specific equipment[25] and are mostly aimed towards obtaining films. In this work, we present a green synthesis method for $Bi_{19}S_{27}I_3$ nanostructures, using the hot injection method under mild conditions and water as the solvent. This method is generally used to synthesize nanoparticles mainly in organic media, very common for quantum dots,[26,27] leading to larger waste generation. However, it has also been used to produce nanostructures of binary semiconductors, such as sulphides.[28] The advantages of this method are many over other syntheses commonly used for semiconductor nanocrystals, such as solvothermal: reaction times are usually lower, one can observe changes in colour in real time, and, most importantly, it is not a one-pot synthesis so there is finer control of how the precursors react. Moreover, most of the reports in hot injection are for binary compounds, and having a ternary compound adds a layer of complexity in the reaction. Using polyethylene glycol (PEG) as a capping agent and varying the reaction time, we could control the morphology of the nanostructures, obtaining either round nanoparticles or nanorolls, or a mixture of both. We also saw that the capping effect proved important when studying this nanomaterial for photocatalysis of Cr(VI). By tuning a simple and fast synthesis method such as the one proposed here, we can engineer the morphology of $Bi_{19}S_{27}I_3$ and test it for the photocatalysis of Cr(VI) with success,

María Eugenia Pérez Barthaburu

María Eugenia Pérez, who holds a PhD in Chemistry, has dedicated her research to the field of nanotechnology with a focus on sustainable development. As a Professor at Universidad de la República in Uruguay, she has effectively combined her expertise in research, teaching, and community engagement. Her interdisciplinary research approach has led to significant contributions in the development of semiconductor nanomaterials for various applications including photocatalysis, solar cells, radiation detection, radiosensitization, photodynamic therapy, and the assessment of ecological impacts of nanoparticles. She has garnered notable achievements particularly in the synthesis and characterization of Hg, Sn, and Bi halides and chalcohalides nanostructures. Beyond her research, she serves as a mentor to aspiring scientists, providing guidance to undergraduate and graduate students, as well as high school teachers.

Ivana Aguiar

Ivana Aguiar, PhD in Chemistry, is an Associate Professor at Universidad de la República, Facultad de Química, Uruguay. With a profound dedication to fostering a sustainable world, she specializes in synthesizing nanoparticles and exploring their applications, particularly their interaction with various forms of radiation. Ivana has been thoroughly involved with the Materials Science and Technology community through her participation in research societies, and has established a network of collaborations to develop interdisciplinary research topics in her country. She has also been instrumental in organizing the first two Materials Science Researchers Meetings in Uruguay. Alongside her teaching responsibilities in materials science and nanotechnology, she actively engages in outreach activities to connect with the wider community.

reaching 91% of degradation in 255 min for the best sample. The use of $Bi_{19}S_{27}I_3$ nanostructures for the photocatalytic reduction of Cr(VI) is motivated by their superior photocatalytic activity, environmental safety, versatility and scalable synthesis methods, cost-effectiveness, and adaptability for enhanced performance. These attributes make $Bi_{19}S_{27}I_3$ nanostructures a promising and environmentally friendly choice for addressing the critical issue of Cr(VI) contamination in water.

2. Experimental

Nanostructure synthesis

The hot injection solution method was chosen for the synthesis of $Bi_{19}S_{27}I_3$, varying the amount of capping agent and the reaction time. $BiCl_3$ (>98%, Merck), thioacetamide (98%, Sigma-Aldrich), and NH_4I (>99% Sigma-Aldrich) were used without further purification. Briefly, $BiCl_3$ was dissolved in Milli-Q water at a concentration of 0.021 mol L^{-1}, and 10 mL of this solution was placed in a round bottom flask. Concentrated HCl (36%, Dorwill) was added dropwise until complete dissolution of $BiCl_3$. Polyethylene glycol, average M_n 400 (PEG 400, Sigma Aldrich) was also added in this step when a capping agent was used. The round flask was put in an oil bath on a stirring hot plate at 136 °C, with a reflux on top. Furthermore, two solutions in Milli-Q water were prepared: thioacetamide (with a concentration of 0.090 mol L^{-1}) and NH_4I (with a concentration 0.063 mol L^{-1}). Once the temperature of the $BiCl_3$ solution was reached, 5 mL of both S and I precursor solutions were consecutively injected at room temperature and left for a determined amount of time. The black powder obtained was separated from the reaction medium by centrifugation at 4025 g for 5 minutes. The washing procedure was as follows: 10 mL of EtOH was added to a Falcon tube containing the solid, followed by 30 seconds of vortex mixing, followed by centrifugation under the conditions described above. The EtOH was discarded afterwards. These steps were repeated 5 times. Then it was air dried at 60 °C for 24 h. After the samples were dried, the powder was lightly ground on an agate mortar only to disaggregate clumps, and stored in glass vials at room temperature under ambient conditions.

All samples were prepared and characterized twice, except in cases where the synthesis had to be repeated multiple times to obtain a sufficient quantity of the product for the photocatalysis experiments. Table 1 summarizes the conditions tested.

Table 1 Synthesis conditions. The sample codes were established as follows: TX_YP, where T is the time, X is the reaction time in minutes; P is PEG as the capping agent, and Y is the molar ratio of PEG related to bismuth

Sample	Time (min)	Capping agent	PEG : Bi	[PEG] (mol L^{-1})
T5_0P	5	—	—	—
T270_0P	270	—	—	—
T5_0.5P	5	PEG	0.5 : 1	0.005
T5_1P	5	PEG	1 : 1	0.011
T5_2P	5	PEG	2 : 1	0.022
T270_0.5P	270	PEG	0.5 : 1	0.005
T270_1P	270	PEG	1 : 1	0.011
T270_2P	270	PEG	2 : 1	0.022

Nanostructure characterisation

Samples were characterized by powder X-ray diffraction (XRD) in a PANalytical Empyrean diffractometer equipped with a Cu Kα source (λ = 1.5418 Å), and the sample holder used was a Si zero background holder. The diffractograms were refined through the Rietveld refinement method (using GSAS-II software[29]) to determine the composition of the samples. Scanning electron microscopy (SEM) (JEOL 5900 Low Vacuum) was employed to determine the morphology and size distribution. Sample preparation for SEM consisted of lightly dropping a small amount of powder onto a double sided carbon taped metal stub, and gently tapping out the excess. Scanning transmission electron microscopy (STEM) with an Oxford Instruments EDS probe was also used to determine the local morphology and composition at higher magnifications. The microscope was a Jeol 2100 with a LaB_6 electron source. The specimens were prepared by suspending approximately 0.005 g of the dry powdered sample in 500 μL of EtOH with the help of sonication for 1 minute, and 5 μL of this suspension was drop cast onto a carbon-coated copper grid. Image processing was carried out using ImageJ software.[30] Calibrated images were used to manually measure the dimension of the particles. A minimum of 500 particles or nanorolls were measured for each sample. The different morphologies were manually counted using the cell count tool. Fourier transform infrared (FTIR) diffuse reflectance spectroscopy (Shimadzu IRPrestige-21 instrument, with a diffuse reflectance DiffusIR Pike Technology accessory), was employed to study the capping agent presence in the samples. Finally, diffuse reflectance UV-vis spectroscopy was used to determine the experimental band gap of the products (using a Shimadzu UV 2600 spectrophotometer equipped with an integrating sphere accessory, employing Spectralon's scatter profile as the reference). The band gap was estimated through the Tauc plot method by mathematical linear fitting of the slope in the graph.[31]

Photocatalysis experiments

We evaluated the photocatalytic capacity of $Bi_{19}S_{27}I_3$ nanorolls against a low Cr(VI) concentration. Samples with and without capping agent (samples T270_0P and T270_1P) were used to reduce the Cr(VI) to Cr(III) under visible light irradiation. The diphenylcarbazide method was employed to follow the process.[32] The experiments were performed in a home-made Pyrex glass photocatalytic reactor of 250 mL capacity attached to a solar simulator SUN 3000 1.5 AMG Abet Technologies with a cutoff filter at 340 nm (Xe lamp 500 W). The reactor allowed magnetic stirring of the solution and was equipped with a refrigeration system to maintain the temperature constant. The distance between the light source and the reactor system was kept constant in all the experiments. For the tests, we mixed 50 mL of a solution of $Na_2Cr_2O_7{\cdot}2H_2O$ with a concentration of 2 mg L^{-1} with 10 mg of photocatalyst. To allow the adsorption equilibrium, the system was kept in the dark with stirring for

30 min. After this time, we irradiated the system, and we took portions of 4 mL at different times, controlling the pH at these intervals using a pH meter (Hanna HI 2210). The fractions were centrifuged at 4000 rpm for 5 minutes. The supernatants were treated according to the aforementioned method, using diphenylcarbazide as the color developer for Cr(VI) and analyzed by UV-vis spectrometry in a Thermo Scientific Genesys 150 spectrometer at 540 nm.

3. Results and discussion

$Bi_{19}S_{27}I_3$ nanostructures

The syntheses using the salt precursors of Bi^{3+} and I^-, and thioacetamide as the sulphur precursor, yielded in all cases $Bi_{19}S_{27}I_3$, as can be seen in the XRD patterns in Fig. 1a and b. The Rietveld refinement of the most crystalline sample, namely T270_0P, is shown in Fig. S1 in the ESI,† resulting in cell parameters a = 15.661 Å and c = 4.024 Å. However, there are differences between the diffractograms that correlate the crystallinity of the sample with the morphologies obtained for the different synthesis conditions. As observed from electron microscopy analysis, two morphologies were obtained: nanorolls and round nanoparticles; images of both morphologies are shown in Fig. 1c and d, the latter depicting a nanoroll in more detail. This morphology is, to the best of our knowledge, the first reported, since $Bi_{19}S_{27}I_3$ has been reported to grow as nanorods,[15,23] tubule-like nanorods[24] and flower-like nanostructures.[22]

A closer inspection of both morphologies was performed using TEM and HR-TEM. For round nanoparticles, high resolution was barely achievable at the edges due to size, rendering the study of local crystallinity for this morphology extremely difficult; this can be observed in Fig. S2 in the ESI.† However, in the case of nanorolls, their particular morphology and their size allowed HR-TEM analysis to be carried out. In these images (Fig. 1d is a representative sample), it is possible to notice that the nanostructures are formed by thin layers of the compound rolled on top of each other, hence the name we have given to them in this article. HR-TEM imaging of a nanoroll, as shown in Fig. 1e, allowed for crystalline plane determination, corresponding to the $Bi_{19}S_{27}I_3$ phase according to the PDF File 73-1157.

Additionally, the local chemical composition could be estimated by EDS through STEM (Fig. S3 in the ESI†). Remarkably, both nanorolls and round nanoparticles exhibited a Bi : S : I ratio close to 19 : 27 : 3, indicative of the presence of $Bi_{19}S_{27}I_3$. However, it is important to note that these values are estimates due to the spectral overlap of the main peaks for Bi and S, leading to potential underestimation of sulfur content. These findings provide further evidence supporting the identification of both round nanoparticles and nanorolls in $Bi_{19}S_{27}I_3$. In the subsequent paragraphs, we will delve into the variations introduced during the synthesis process, namely alterations in synthesis time and the quantity of capping agent employed.

First, for sample T5_0P, the XRD diagram corresponds to $Bi_{19}S_{27}I_3$ according to the PDF file 73-1157 and is shown in Fig. 1a. After 5 minutes of reaction, the $Bi_{19}S_{27}I_3$ comprises nanorolls and nanoparticles (Fig. 2 left), obtaining approximately 50% nanorolls and 50% nanoparticles as is shown in Fig. 3c. When the reaction time is extended to 270 min (sample

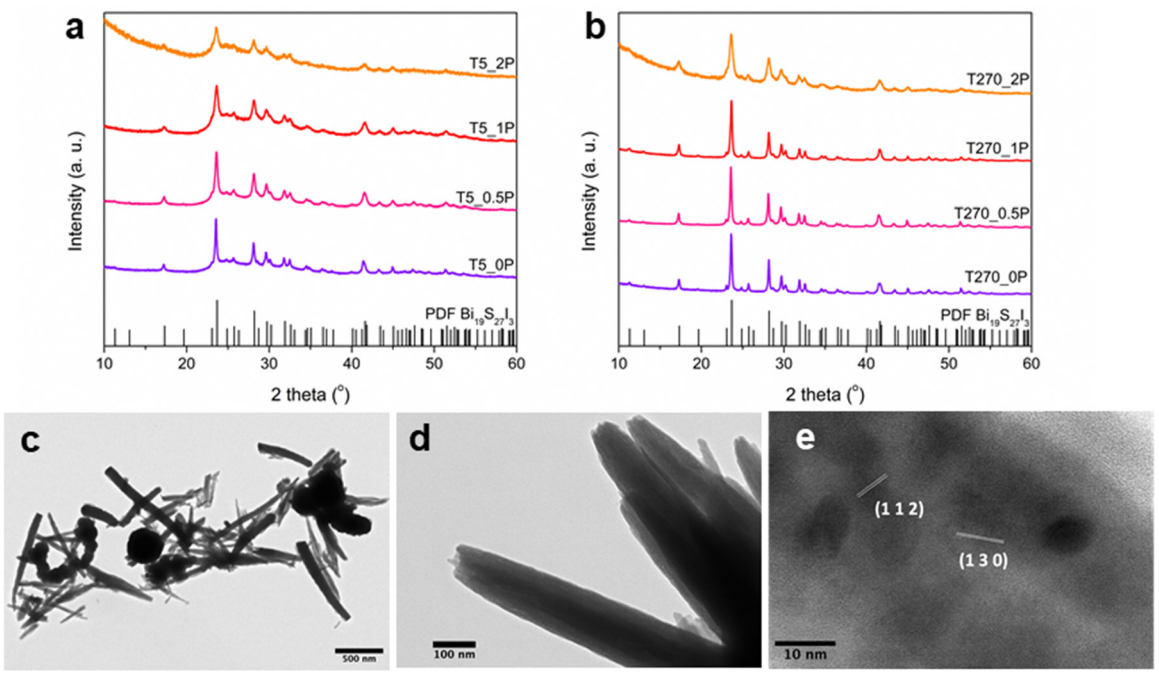

Fig. 1 (a) XRD diagrams of the samples synthesized with a time of 5 min, (b) XRD diagrams of the samples synthesized with a time of 270 min, (c) TEM image of a representative sample synthesized with PEG (T5_1P), with nanorolls and round nanoparticle morphologies, (d) TEM image of nanorolls, and (e) HR-TEM image of a nanoroll.

T270_0P), the round nanoparticles disappear and the sample only presents nanorolls, as shown in Fig. 2 (right). The median of the nanorolls is 173 ± 35 nm for 5 min and 186 ± 38 nm for 270 min (see Fig. 3a and Table S1 in the ESI†). Thus, the nanorolls do not grow when using longer reaction times.

With a 93% reaction yield for the 5 minute reaction and a 52% reaction yield for the 270 min reaction (as is shown in Fig. 3e), one could conclude that extending the reaction time promotes the dissolution of the round nanoparticles. Therefore, the dissolved entities do not contribute to the nanoroll growth. It is noteworthy that the XRD diagrams differ in their background as well, with the sample from the shorter reaction time having two distinct regions with higher background signal (from here on referenced as "background bellies") between 25–35° and 40–50°, which could be due to an amorphous component of the round nanoparticles.

When PEG was added to the reaction mixture, the size and predominant morphology of the nanostructures in the samples were affected. For 5 minutes of reaction time, the variation in PEG concentration has several influences on the resulting $Bi_{19}S_{27}I_3$ nanostructures. The first observation worth noticing is the XRD characterisation at low 2 theta values, where a higher background is correlated with a higher content of PEG (Fig. 1a, sample T5_2P with a PEG : Bi ratio of 2 : 1). Furthermore, all diffractograms, in this case, present the background bellies mentioned in the section above, but it is considerably more noticeable for the sample with the highest amount of PEG used in the reaction. Regardless of the amount of PEG used, both nanorolls and round nanoparticles are present after 5 minutes of reaction time. However, there is a difference in their quantities, as can be seen in Fig. 3c. When the amount of PEG is

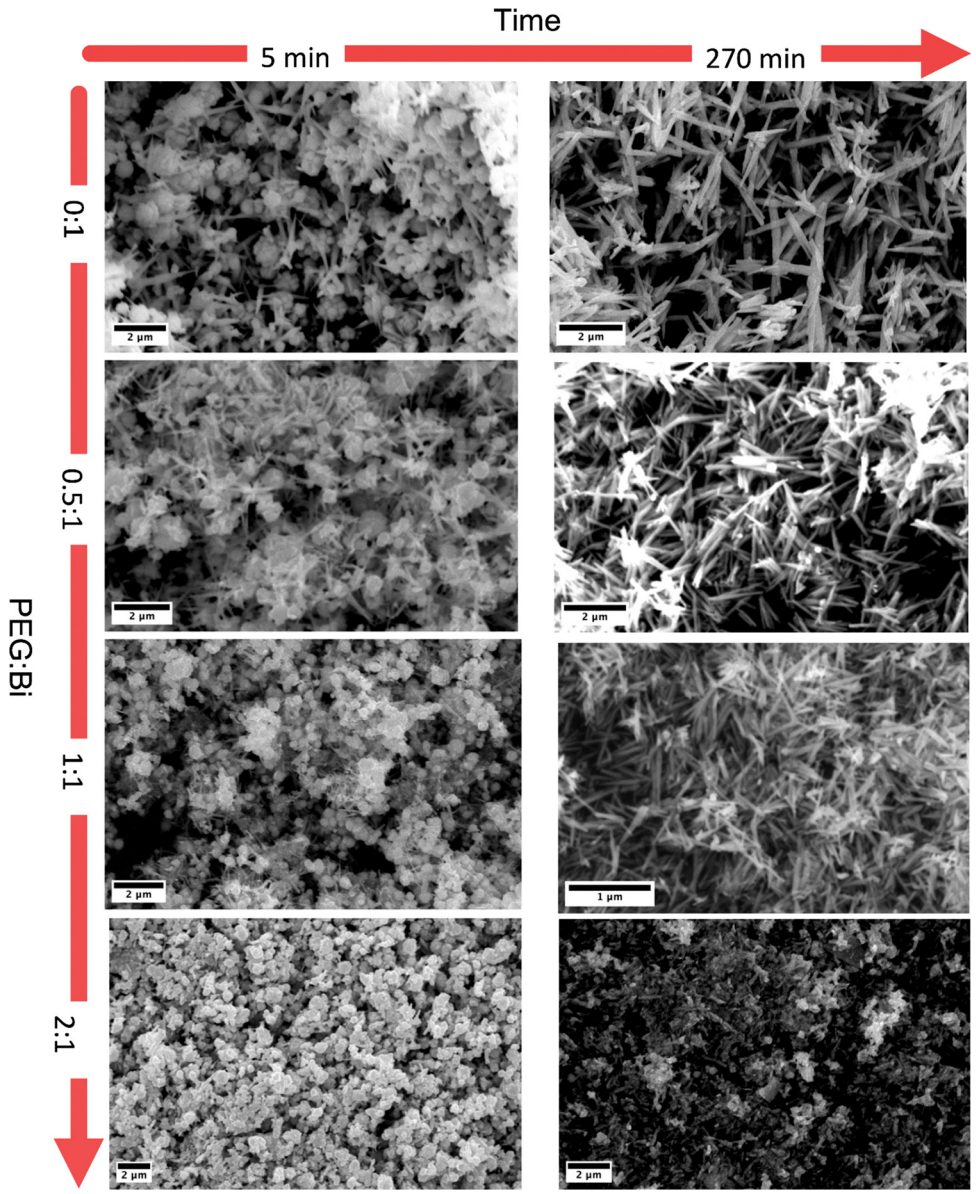

Fig. 2 SEM images of the samples synthesized at different reaction times and with different PEG : Bi ratios.

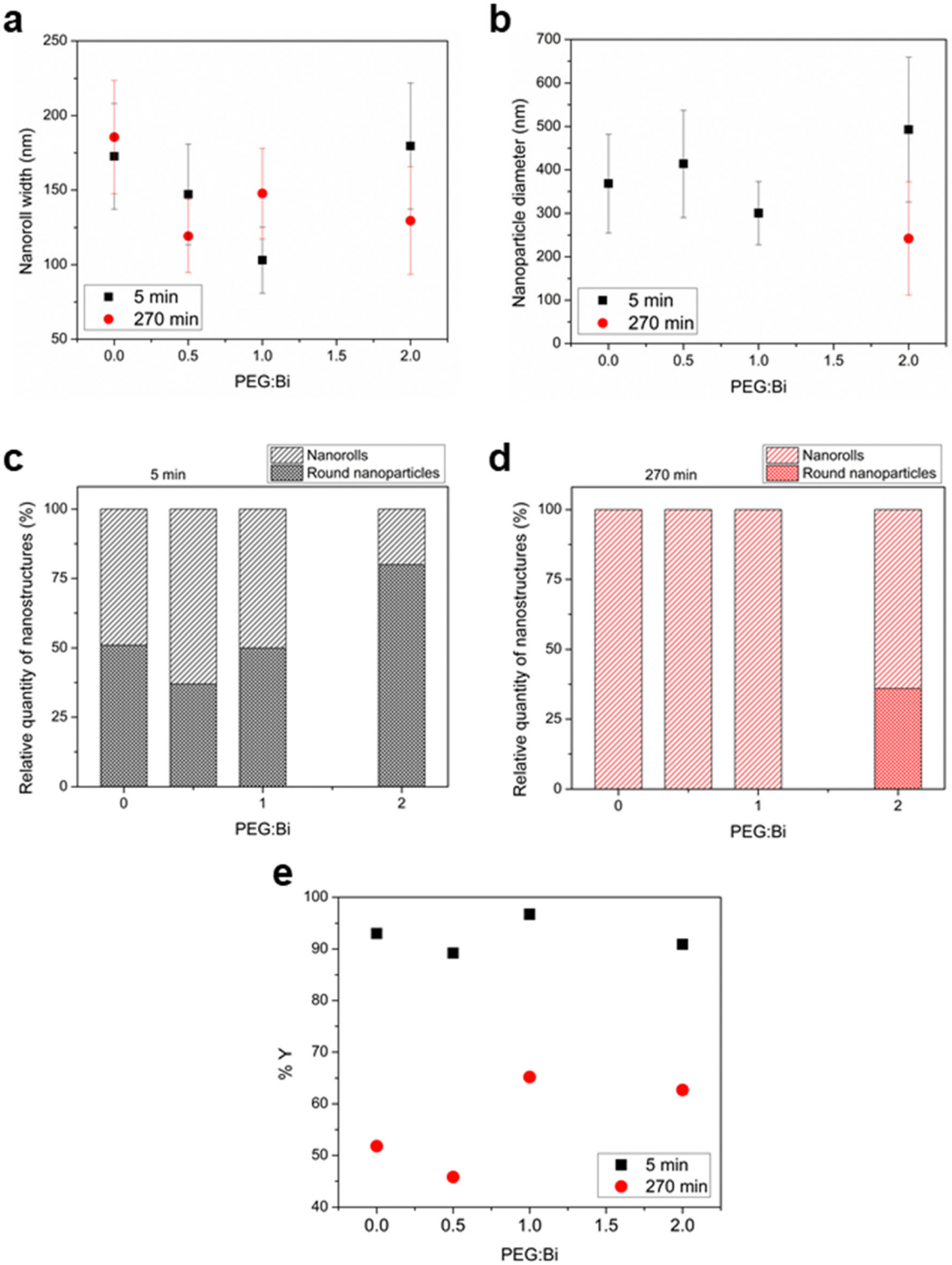

Fig. 3 Variation of parameters *vs.* PEG : Bi ratio. (a) Nanoroll sizes with different synthesis times, (b) nanoparticle sizes with different synthesis times, (c) quantity of nanorolls and nanoparticles with a 5 min synthesis time, (d) idem *c* for the 270 min synthesis time, and (e) reaction yields.

increased to a ratio of 2 : 1 with regard to Bi, most of the sample presents round nanoparticles, and only some nanorolls are observed (Fig. 2, bottom-left), while with no PEG, the amount of nanorolls is considerably higher (Fig. 2, above-left). The correlation between the amount of round nanoparticles and the diffractogram profile is further evidence of the partially amorphous nature of round nanoparticles.

If we extend the reaction time to 270 min, only with a PEG : Bi ratio of 2 : 1 round nanoparticles are present, while for lower quantities of PEG there are only nanorolls (as shown

in Fig. 2, right). The higher intensity of the XRD diffraction peaks with no background in the 20–35° region for 270 min in all cases indicates a higher degree of crystallinity, and can also be related to the absence of round particles. Moreover, in all samples with a reaction time of 270 minutes, the reaction yield is considerably lower than for 5 minutes, which should be taken into account for future applications. Therefore, the less stable round nanoparticles dissolve with longer reaction times.

Concerning the effect of PEG as the capping agent, the 50–50% ratio of nanorolls and round nanoparticles is maintained up to a PEG : Bi ratio of 1 : 1. The size of nanorolls (for 5 min of reaction) decreases as the PEG : Bi ratio increases. However, the diameter of the nanoparticles remains unchanged, indicating a slight capping effect on the crystalline part of the material, that is to say the nanorolls. Over time, the nanoparticles dissolve again, and the nanorolls either remain largely unchanged or show a minimal decrease in size. When we employed a PEG : Bi ratio of 1 : 1, the nanorolls were minimized in size, and the nanoparticles were relatively unchanged until their dissolution at 270 min, indicating once more a capping effect on the crystalline part of the sample. With a 2 : 1 ratio, we observe almost an 80% presence of round nanoparticles and a lower proportion of larger nanorolls.

FTIR spectroscopy was conducted to delve deeper into the interaction between PEG and $Bi_{19}S_{27}I_3$. Fig. 4 (left and right) show the spectra of the samples for 5 minutes and 270 minutes of reaction, respectively, compared with PEG. In the samples synthesized during 5 minutes, four principal bands ascribed to PEG were found, and three of them are present only in samples with a higher PEG : Bi ratio,[33] namely T5_1P and T5_2P. While the C–O group at 1070–1110 cm^1 is present in all the samples, the following bands were identified exclusively in the samples with a higher PEG content: the C–H sp^2 band at ~800 cm^{-1}, the C–OH group at ~1280 cm^{-1}, and the C–H sp^3 band at ~1450 cm^{-1}. The band between 1627–1660 cm^{-1} is attributed to the deformation bands associated with water content.[34] Considering the sizes and quantities of the nanostructures discussed above, it is revealed that the PEG is not only present in the samples but it evidently acts as a capping agent. However, when we performed the FTIR spectra with the samples synthesized for 270 min, we observed that some of the peaks of the PEG disappeared. As we determined that PEG is responsible for the round morphology, and the round particles dissolve after 270 minutes of reaction, it is possible that a portion of the PEG is lost during the prolonged reaction time and subsequent washing.

Thermogravimetric analysis (TGA, Fig. 5a) and differential scanning calorimetry (DSC, Fig. 5b) were carried out to complement the FT-IR characterization. The weight loss between 300 and 500 °C in all thermograms is indicative of PEG presence, as a weight loss in this temperature range is also observed in the thermogram of pure PEG (Fig. S4 in the ESI†). There is a clear effect of the reaction time in the PEG content on the resulting nanostructures, given by the comparison of the thermograms of the sample without PEG (T270_0P) with only a 3% weight loss, and the other samples with PEG in the reaction medium (the error in the weight loss percentage is 2%). The first observation is that

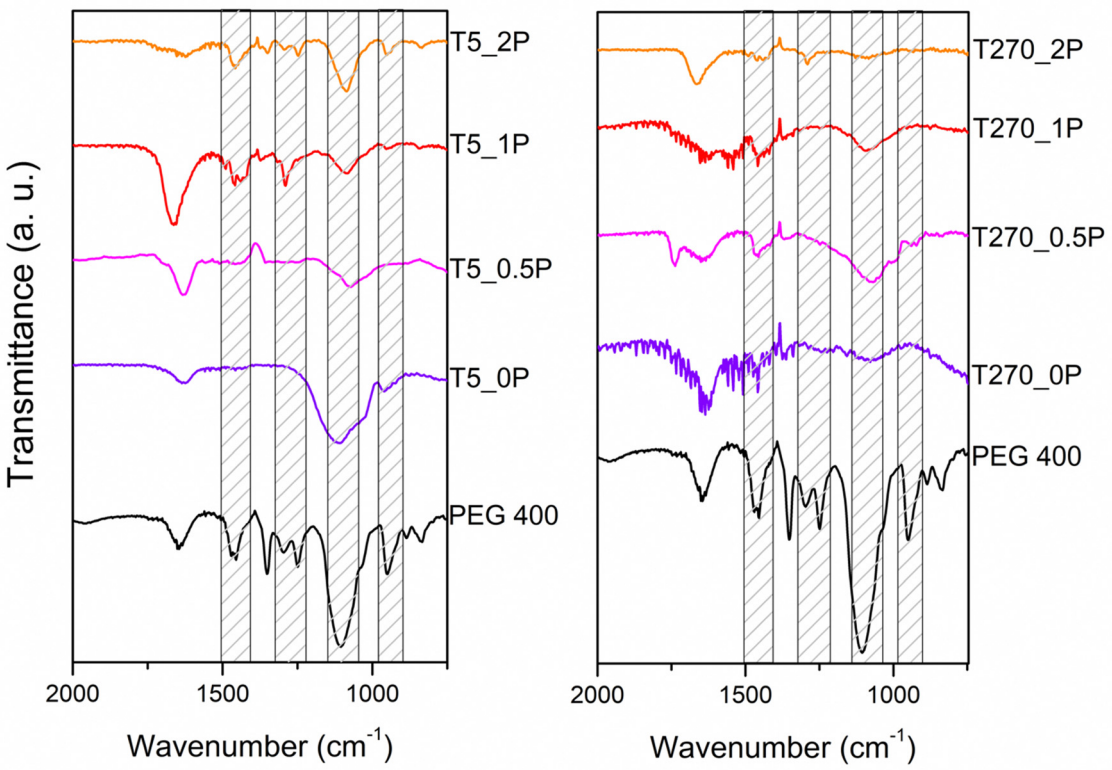

Fig. 4 FTIR spectra of the $Bi_{19}S_{27}I_3$ samples compared with PEG 400 for 5 and 270 minutes of reaction. The bands of interest are marked in both graphs.

overall, shorter reaction times have a greater weight loss than longer reaction times, for all samples regardless of the content of PEG. Within the same reaction time, the weight loss increases with increasing amount of added PEG. This is further proof that the capping interaction with PEG is successful at short reaction times, promoting the formation of round particles, which once the reaction progresses to longer times, dissolve in the media, releasing the PEG, which is in turn washed away in the solid processing once the synthesis is completed. There is a distinct difference for the 270 minutes of reaction with a 2 : 1 PEG : Bi molar ratio synthesis sample, in that it suffers a higher weight loss. This sample contains round particles, unlike the others synthesized with this time, which are only comprised of nanorolls. As for the DSC, there is an event present in all samples at 5 minutes of reaction time at around 200 °C, which for the longer reaction time this even is only noticeable, albeit barely, for the sample with highest PEG content. Once again, all of these samples are the ones that contain round particles as well as nanorolls.

The smallest nanostructures (both nanorolls and round nanoparticles) obtained with a PEG : Bi ratio of 1 : 1 and 5 minutes of reaction, indicate that at this concentration, the PEG has the best capping effect to limit the nanostructure growth of $Bi_{19}S_{27}I_3$ in both morphologies and stay bound to them, whereas for 270 min the PEG influence is not as strong and the nanorolls experience a slight growth. Additionally, when a 0.5 : 1 ratio is used, the concentration of PEG does not seem to be enough in the reaction volume to have a successful interaction with the growing nanostructures. Finally, for a 2 : 1 ratio, the PEG present can be in excess and the high concentration and heat can favor the inter-polymer interaction and prevent an efficient interaction with the growing nanocrystals. This kind of effect of PEG concentration for nanoparticles has already been reported for other materials.[35]

Optical properties

In this investigation of the photocatalytic properties of $Bi_{19}S_{27}I_3$, we focused on the crystallinity of the samples, their morphology, and the presence of a capping agent. Specifically, we selected two samples, T270_1P and T270_0, comprised solely of crystalline nanorolls, synthesized with and without PEG, respectively. The determination of the band gap of these samples was conducted *via* diffuse reflectance UV-vis spectroscopy (Fig. 6a), employing the Kubelka–Munk transformation and plotting the Tauc function[31] (Fig. 6b), and considering a direct band gap as has been already documented.[15] Our analysis yielded a consistent band gap value of 1.00 eV for both samples, aligning closely with findings in the existing literature. Various authors have previously reported band gap values of 1.15 eV,[22] 0.91 eV,[24] 1.08 eV,[36] and 0.83 eV,[15] further validating our results.

Photocatalytic properties

The relative concentration C/C_0 (where C is the concentration at time t and C_0 is the initial Cr(VI) concentration) *versus* time for each sample is shown in Fig. 7. As can be seen, not only is there a different behavior in how the nanorolls catalyze the degradation for Cr(VI), given by the differences in the curves, but the sample with PEG T270_1P is more efficient in the degradation of Cr(VI) under the same conditions compared with T270_0P, which is the sample without PEG. With 91% degradation compared with 45% after 255 minutes, the superior yield of T270_1P is irrefutable. The calculated apparent rate constant (k), using a pseudo-first-order kinetic, is 0.01 min^{-1} for this nanomaterial. If we compare our results with other reported values for bismuth based semiconductors containing sulfur and halides (Table 2), most reports use a five-fold or higher concentration of Cr(VI), and it has been determined that the photocatalysis yield is better at higher Cr(VI) concentrations.[37] Our study focuses on low Cr(VI) concentrations as a first approach, indicating that these preliminary results can only be improved further, not only for pure $Bi_{19}S_{27}I_3$, but with heterostructures, for example.

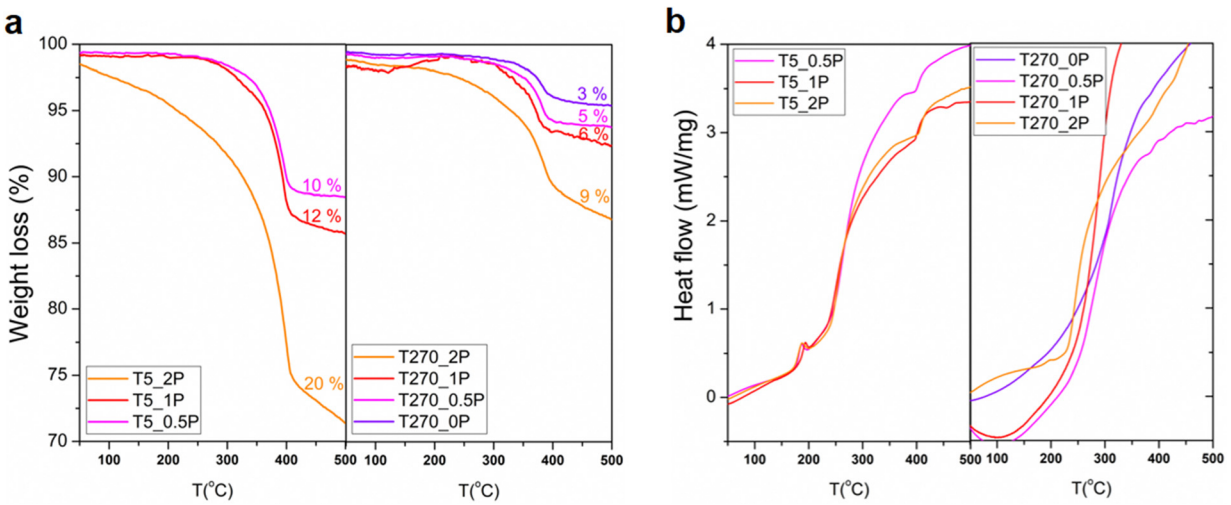

Fig. 5 (a) Thermogravimetric analysis of the synthesized samples of $Bi_{19}S_{27}I_3$ at different reaction times and PEG : Bi molar ratios. (b) Differential scanning calorimetry of the synthesized samples of $Bi_{19}S_{27}I_3$ at different reaction times and PEG : Bi molar ratios.

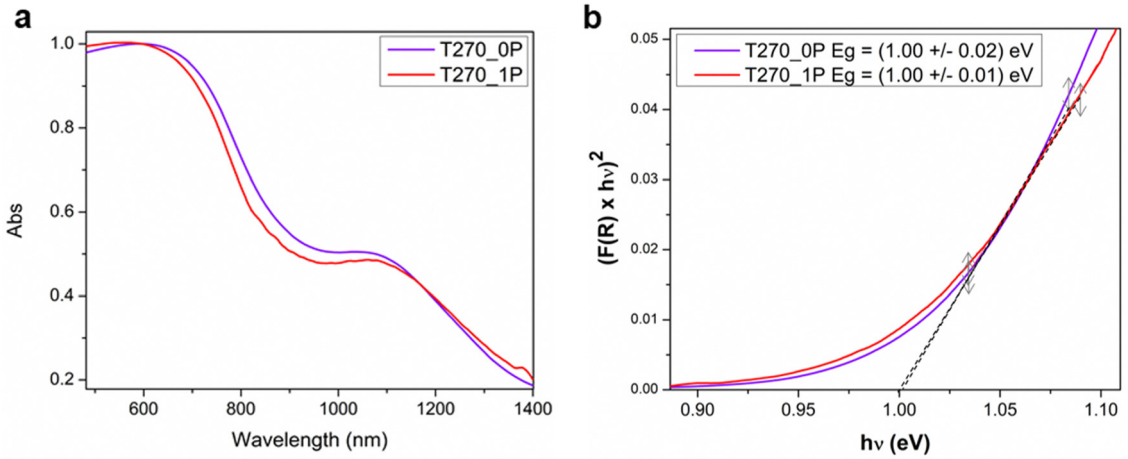

Fig. 6 (a) UV-vis absorption spectra of the T270_0P and T270_1P samples. (b) Tauc plot after Kubelka–Munk transformation for the direct band gap of $Bi_{19}S_{27}I_3$ in samples T270_0P and T270_1P. Calculated values are shown with the error of fitting.

In order to investigate whether the reduction of Cr(VI) occurs through direct transfer from the semiconductor to the species, we determined the conduction band position (E_{CB}) of the samples using the following equation:[4,42]

$$E_{CB} = E^e - X + \frac{1}{2}E_g$$

where E^e is the energy of free electrons in the hydrogen scale (4.44 eV) and X is the absolute electronegativity of the semiconductor expressed as the geometric mean of the Mulliken electronegativity of the constituent atoms. E_{VB} was obtained through $E_{VB} = E_{CB} + E_g$. We obtained $E_{CB} = -0.66$ eV and $E_{VB} = 0.34$ eV (*vs.* NHE). Comparing the E_{CB} value with the reduction potential of Cr(VI)–Cr(III) (0.51 eV), it can be inferred that the reduction occurs through direct electron transfer. Additionally, a proportion of the generated electrons can react with the adsorbed O_2 promoting further Cr(VI) reduction.

Considering the fact that in both samples the only difference is the PEG present, we must rule out a difference in exposed surface due to nanoroll size, for instance. However, an important observation was made when the photocatalysis was carried out. As shown in Fig. 8a, the PEG-capped nanorolls are considerably better suspended in water than the non-PEG-capped ones, which aggregate forming large clusters. While one could think the PEG covering the surface of the nanorolls would act negatively in the charge transfer between $Bi_{19}S_{27}I_3$ and Cr(VI), in the synthesis conditions employed for T270_1P, the PEG is just enough for the stabilization of the nanorolls in an aqueous solution, allowing for a more intimate exchange between the semiconductor nanostructure surface and the cations in solution.

Another important aspect to highlight is the working pH. In our photocatalysis, the pH was between 5.2 and 5.5 throughout the experiment. It is well known that Cr(VI) reduction is favored at an acidic pH, but many photocatalytic materials undergo corrosion under these conditions.[13] $Bi_{19}S_{27}I_3$ is stable in an acidic medium, and further studies should be carried out at lower pH values to determine the optimum pH for photocatalysis, giving it an additional advantage for treating water contaminated with Cr(VI).

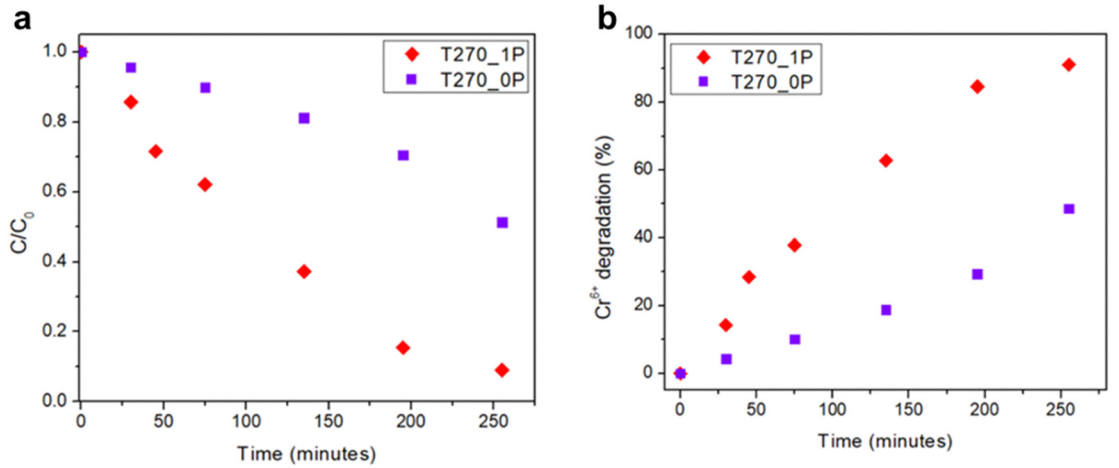

Fig. 7 (a) Cr(VI) reduction using $Bi_{19}S_{27}I_3$ synthesized with and without PEG as the capping agent as photocatalysts, and (b) variation in the % of Cr(VI) reduction over time.

Table 2 Comparison of the photocatalysis parameters for different bismuth-based compounds

Photocatalyst	Cr(VI) concentration (mg L^{-1})	Lamp source	Catalyst dosage (mg L^{-1})	Light application time (min)	Removal rate (%)	Ref.
$(Bi_{19}S_{27}I_3)_{0.6667}$	10	300 W xenon lamp	200	60	94.1	38
Bi_2S_3	20–100	—	100	90	~90	39
BiSI	20	300 W xenon lamp	1000	30	~100	17
BiOBr–Bi_2S_3	10	500 W xenon lamp	500	12	100	40
Bi_2S_3/BiOBr	30	Halogen, 50 W	1000	60	74.3	41
$Bi_{19}S_{27}I_3$	2	500 W xenon lamp	200	250	91	This paper

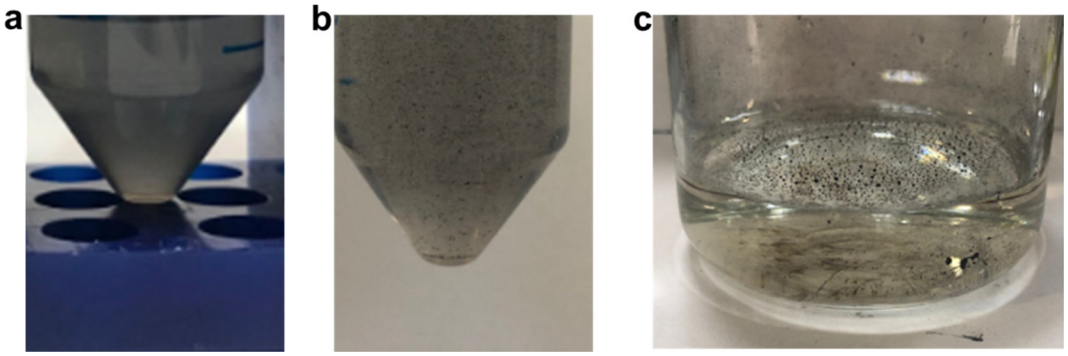

Fig. 8 (a) Sample T270_1P suspended in Cr(VI) aqueous solution in a falcon tube; (b) sample T270_0P suspended in Cr(VI) aqueous solution in a falcon tube; (c) sample T270_0P in Cr(VI) aqueous solution in the photocatalysis reactor.

4. Conclusions

This work presents a green synthesis approach for nanostructures of $Bi_{19}S_{27}I_3$, utilizing water as a solvent and low temperatures, thus reducing energy costs. Additionally, we have successfully controlled the morphology of the nanostructures by adding PEG as the capping agent at different concentrations and varying the reaction time, to obtain a mixture of nanorolls and round nanoparticles, or only nanorolls. We have seen that longer reaction times such as 270 min enhance the crystallinity of the material and also encourage morphology uniformity, while the PEG favors the rounded morphology. Furthermore, the incorporation of a capping agent improved the nanostructure dispersion in water, boosting the $Bi_{19}S_{27}I_3$ efficiency of the nanostructures as a photocatalyst for low concentration Cr(VI) reduction in aqueous environments. This paper contributes to advancing the state of the art in promising semiconductor nanomaterials, with ample room for fine tuning $Bi_{19}S_{27}I_3$ properties, particularly for water purification applications. Additionally, the report of an easily synthesized new morphology paves the way for exploring diverse technological applications.

Author contributions

Maia Mombrú-Frutos: conceptualization, methodology, formal analysis, writing – original draft, and writing – review & editing. Martina Viera: investigation, methodology, and formal analysis. Carolina Grosso: investigation and methodology. Mauricio Rodríguez Chialanza: TG/DSC analysis. Laura Fornaro: visualization and writing – review and editing. María Perez Barthaburu: conceptualization, methodology, supervision, visualization, funding acquisition, writing – original draft, and writing – review & editing. Ivana Aguiar: conceptualization, data curation, formal analysis, methodology, visualization, funding acquisition, supervision, writing – original draft, and writing – review & editing.

Data availability

Data for this article, including XRD, FTIR, size measurement, UV-vis, TG/DSC and photcatalysis data are available at Redata at **https://doi.org/10.60895/redata/NH8BDS**.

Conflicts of interest

There are no conflicts to declare.

Acknowledgements

The authors want to thank the Comisión Sectorial de Investigación Científica from Universidad de la República, Agencia Nacional de Investigación e Innovación (ANII), grant FCE_3_2016_1_126475 and the Programa de Desarrollo de las Ciencias Básicas for funding. They also acknowledge Isabel Galain from Área Radioquímica, Departamento Estrella Campos, Facultad de Química, Udelar, for the DLS measurements, Alexandra Sixto from Área Química Analítica, Departamento Estrella Campos, Facultad de Química, Udelar, for her help in the Cr(VI) determination; Alvaro Olivera from Laboratorio de Alta Resolución, Departamento de Desarrollo Tecnológico, CURE,

Udelar, for the TEM images and analysis; H. Bentos Pereira from Departamento de Desarrollo Tecnológico, CURE, Udelar, for the XRD measurements; and Laboratorio de Fisicoquímica, Facultad de Química, Udelar, for the FTIR equipment.

References

1 K. E. Ukhurebor, U. O. Aigbe, R. B. Onyancha, W. Nwankwo, O. A. Osibote, H. K. Paumo, O. M. Ama, C. O. Adetunji and I. U. Siloko, *J. Environ. Manage.*, 2021, **280**, 111809.
2 B. Qiu, C. Xu, D. Sun, Q. Wang, H. Gu, X. Zhang, B. L. Weeks, J. Hopper, T. C. Ho, Z. Guo and S. Wei, *Appl. Surf. Sci.*, 2015, **334**, 7–14.
3 K. Gong, Q. Hu, L. Yao, M. Li, D. Sun, Q. Shao, B. Qiu and Z. Guo, *ACS Sustainable Chem. Eng.*, 2018, **6**, 7283–7291.
4 D. Oreggioni, A. Pérez Parada, I. Aguiar, M. Colazzo, L. Pareja, M. A. De León, H. B. Pereira and M. E. Pérez Barthaburu, *Environ. Sci. Pollut. Res.*, 2021, **28**, 18234–18245.
5 M. Ao, X. Chen, T. Deng, S. Sun, Y. Tang, J. L. Morel, R. Qiu and S. Wang, *J. Hazard. Mater.*, 2022, **424**, 127233.
6 T. L. DesMarias and M. Costa, *Curr. Opin. Toxicol.*, 2019, **14**, 1–7.
7 R. A. Anderson, *Regul. Toxicol. Pharmacol.*, 1997, **26**, S35–S41.
8 Guidance. Chromium: toxicological overview. United Kingdom government, **https://www.gov.uk/government/publications/chromium-general-information-incident-management-and-toxicology/chromium-toxicological-overview#references**, accessed 25th July 2024.
9 D. Rai, B. M. Sass and D. A. Moore, *Inorg. Chem.*, 1987, **26**, 345–349.
10 L. Wang, N. Wang, L. Zhu, H. Yu and H. Tang, *J. Hazard. Mater.*, 2008, **152**, 93–99.
11 X. Niu, J. Dong, X. L. Wang and Y.-F. Yao, *Environ. Sci.: Nano*, 2020, **7**, 2823–2832.
12 M. Ijaz and M. Zafar, *Int. J. Energy Res.*, 2021, **45**, 3569–3589.
13 R. Djellabi, P. Su, E. A. Elimian, V. Poliukhova, S. Nouacer, I. A. Abdelhafeez, N. Abderrahim, D. Aboagye, V. V. Andhalkar, W. Nabgan, S. Rtimi and S. Contreras, *J. Water Process Eng.*, 2022, **50**, 103301.
14 V. Hasija, P. Raizada, P. Singh, N. Verma, A. A. P. Khan, A. Singh, R. Selvasembian, S. Y. Kim, C. M. Hussain, V.-H. Nguyen and Q. Van Le, *Process Saf. Environ. Prot.*, 2021, **152**, 663–678.
15 Y. Yan, Y. Xu, S. Lei, X. Ou, L. Chen, J. Xiong, Y. Xiao and B. Cheng, *Dalton Trans.*, 2018, **47**, 3408–3416.
16 M. M. Frutos, M. E. P. Barthaburu, L. Fornaro and I. Aguiar, *Nanotechnology*, 2020, **31**, 225710.
17 J. Liu, J. Wu, N. Wang, F. Tian and J. Li, *Chem. Eng. J.*, 2022, **435**, 135152.
18 J. Xiong, Z. You, S. Lei, K. Zhao, Q. Bian, Y. Xiao and B. Cheng, *ACS Sustainable Chem. Eng.*, 2020, **8**, 13488–13496.
19 Y. Wu, B. Zhou, C. Yang, X. Zhou and W.-H. Zhang, *Chem. Commun.*, 2017, **53**, 5445–5448.
20 D. Tiwari, F. Cardoso-Delgado, D. Alibhai, M. Mombrú and D. J. Fermín, *ACS Appl. Energy Mater.*, 2019, **2**, 3878–3885.
21 H. Kunioku, M. Higashi and R. Abe, *Sci. Rep.*, 2016, **6**, 32664.
22 O. Amiri, F. Beshkar, S. S. Ahmed, A. Rafiei-Miandashti, P. H. Mahmood and A. A. Dezaye, *Adv. Powder Technol.*, 2021, **32**, 1088–1098.
23 S. Li, L. Xu, X. Kong, T. Kusunose, N. Tsurumachi and Q. Feng, *J. Mater. Chem. C*, 2020, **8**, 3821–3829.
24 K. Adams, A. F. González, J. Mallows, T. Li, J. H. J. Thijssen and N. Robertson, *J. Mater. Chem. A*, 2019, **7**, 1638–1646.
25 Z. Li, Q. Zhang, L. Wu, W. Gu and Y. Liu, *Adv. Powder Technol.*, 2019, **30**, 1985–1988.
26 X. Peng, L. Manna, W. Yang, J. Wickham, E. Scher, A. Kadavanich and A. P. Alivisatos, *Nature*, 2000, **404**, 59–61.
27 C. de Mello Donegá, P. Liljeroth and D. Vanmaekelbergh, *Small*, 2005, **1**, 1152–1162.
28 I. A. Isabel Galain, María Cardoso, Emilia Tejería, Gustavo Mourglia-Ettlin, Paula Arbildi, Mariella Terán and María Pérez Barthaburu, *J. Nanopart. Res.*, 2022, **24**, 68.
29 B. H. Toby and R. B. von Dreele, *J. Appl. Crystallogr.*, 2013, **46**, 544–549.
30 C. A. Schneider, W. S. Rasband and K. W. Eliceiri, *Nat. Methods*, 2012, **9**, 671–675.
31 P. Makuła, M. Pacia and W. Macyk, *J. Phys. Chem. Lett.*, 2018, **9**, 6814–6817.
32 A. Wiryawan, R. Retnowati, P. Burhan and S. Syekhfani, *J. Environ. Eng. Sustain. Technol.*, 2018, **5**(1), 37–46.
33 N. S. Vrandečić, M. Erceg, M. Jakić and I. Klarić, *Thermochim. Acta*, 2010, **498**, 71–80.
34 M. Cherecheş, D. Bejan, E. I. Cherecheş and A. A. Minea, *J. Mol. Liq.*, 2022, **356**, 119049.
35 C. Pereira Gomes, V. Leiro, C. D. Ferreira Lopes, A. P. Spencer and A. P. Pêgo, *Acta Biomater.*, 2018, **78**, 247–259.
36 C.-H. Ho, Y.-H. Chen, Y.-K. Kuo and C. W. Liu, *Chem. Commun.*, 2017, **53**, 3741–3744.
37 Y. Sun, J. E. Szulejko, K.-H. Kim, V. Kumar and X. Li, *Chinese J. Catal.*, 2023, **55**, 20–43.
38 L. Ai, L. Wang, N. Guo, M. Xu, D. Jia, C. Tan, X. Jia, W. Cai and Y. Yang, *Int. J. Energy Res.*, 2022, **46**, 23857–23870.
39 D. C. Onwudiwe, O. A. Oyewo, U. Atamtürk, O. Ojelere and S. Mathur, *J. Environ. Chem. Eng.*, 2020, **8**, 103816.
40 Z. Long, G. Zhang, H. Du, J. Zhu and J. Li, *J. Hazard. Mater.*, 2021, **407**, 124394.
41 S. M. El-Sheikh, A. B. Azzam, R. A. Geioushy, F. M. El Dars and B. A. Salah, *J. Alloys Compd.*, 2021, **857**, 157513.
42 M. A. Butler and D. S. Ginley, *J. Electrochem. Soc.*, 1978, **125**, 228–232.